Sol–gel preparation of Zn–V–Mn–O thin films for low voltage varistor applications

Anjan Sil[a], Kiran A.[a], Niranjana A.P.[a], Kevin M. Knowles[b*]

[a] Department of Metallurgical and Materials Engineering,
Indian Institute of Technology Roorkee, Roorkee-247667, India

[b] Department of Materials Science and Metallurgy, University of Cambridge,
27 Charles Babbage Road, Cambridge, CB3 0FS, U.K.

Abstract

ZnO-based thin films in the Zn–V–Mn–O system have been synthesised by a sol–gel process and characterised for use in low voltage varistor applications. The films were prepared through multi-layer deposition of a precursor solution onto indium tin oxide-coated borosilicate glass substrates by spin-coating and subsequent annealing. Current–voltage characteristics measured for the films annealed at 700 °C showed varistor action with nonlinear coefficients (α) above 4.

Keywords: Sol–gel process; thin films; varistor; zinc oxide

* Corresponding author. Tel.: +44 1223 334312

E-mail address: kmk10@cam.ac.uk

1. Introduction

Zinc oxide doped with several different metal oxides acts as a smart semiconducting electronic ceramic material, which exhibits non-ohmic varistor behaviour of a strongly increasing current with increasing voltage [1]. The non-ohmic behaviour of such ceramics is produced through the addition of elements such as Bi, Pr, and Ba with relatively large ionic radii [2]. These varistors are used widely as surge arrestors for overvoltage protection systems ranging in sizes suitable for electronic circuits through to electric power systems [3]. The preparation of bulk zinc oxide-based varistor ceramics requires sintering powders at high temperature, typically in the range 1000–1400 °C [4]. However, multilayered chip components with silver as inner electrode materials limit the sintering temperature to a lower value of about 900 °C because the melting point of silver is 961 °C [5]. Otherwise, expensive metals like palladium or platinum are required.

Amongst the various ceramic varistor families capable of being sintered at relatively low temperatures, one family is based on the $ZnO–V_2O_5$ binary oxide system [5–10]. Electrical circuitry in microelectronic devices and nanodevices require ceramic varistors with low voltage operation, for which thin film technology is suitable [11]. A number of techniques for the preparation of zinc oxide-based thin films such as sol–gel, sputtering, and evaporative deposition have been reported in recent years [11,12]. Of these, sol–gel synthesis offers fine control of composition, microstructure and functional properties of nanostructured zinc oxides and therefore has considerable practical interest for economical, large scale manufacture of zinc oxide-based thin films [11–19]. It also enables films with relatively complex chemistries based on zinc oxide as its main constituent to be made, thus making it particularly suitable for thin film varistors [11].

In the work reported here, sol–gel thin films based on the Zn–V–Mn–O system were prepared from a liquid precursor solution of zinc acetate, manganous acetate and ammonium metavanadate using a spin-coating process [20,21] in which the parameters for film production were optimised. In this coating process, precursor films on the substrates were formed in air at room temperature, after which they were heat treated first to decompose the organic constituents and secondly to crystallise the thin films. Prior work on bulk ceramic varistors based on the Zn–V–Mn–O system has shown that it is a good varistor former in bulk form [5–10, 22–24], but, to the best of the authors' knowledge, varistor thin films based on this chemistry have not been studied or reported. An assessment of the prior work on bulk

material suggested a target composition of ZnO – 0.5mol% V_2O_5 – 1.5mol% MnO as being suitable, since recent work has suggested that manganese is most favourably incorporated in a divalent state into the zinc oxide grains and any minor secondary phases such as the *L* phase [25, 26].

2. Experimental

Zinc oxide-based thin films were prepared by a sol–gel method. Zinc acetate dehydrate ($Zn(CH_3COO)_2.2H_2O$) (Sigma-Aldrich, > 98% purity) was dissolved in a 2-methoxyethanol ($CH_3OCH_2CH_2OH$) (Rankem, 99% purity)–monoethanolamine (MEA: $H_2NCH_2CH_2OH$) (Sigma-Aldrich, > 98% purity) solvent at room temperature. The molar ratio of MEA to zinc acetate was maintained at 1.0. The dopants (manganous acetate tetrahydrate (Aldrich ≥ 99% purity) and ammonium metavanadate (Sigma-Aldrich, > 99% purity)) were dissolved separately in 2-methoxyethanol (Rankem, 99% purity) with the addition of MEA (Aldrich, > 99.5% purity), and stirred with a magnetic stirrer for 20 mins at 70–80 °C. Initial work examined a number of ZnO : MnO : V_2O_5 ratios before a final sol composition was selected in which the relative ratio of the component oxides after annealing was a ZnO : MnO : V_2O_5 ratio of 98.0 : 1.5 : 0.5 in mol%. These relatively high molar ratios of MnO and V_2O_5 were selected to examine the limits of solubility of the pre-prepared dopant solutions in the zinc acetate solution while also being within the Zn–Mn–V–O composition space in which good bulk varistor behaviour is seen [24]. The pre-prepared dopant solutions were added to the zinc acetate solution while maintaining a sol concentration of 1.5 mol l^{-1}. The resultant precursor solution mixture was stirred for 24 h while the temperature of the solution was maintained at 70–80 °C. This produced a clear homogeneous solution. A few drops of ethylene glycol (Rankem, 98% purity) were added to the homogeneous solution to help increase the level of sol viscosity required for the preparation of the precursor film on the substrate. At 20 °C, the viscosity of ethylene glycol is 20.8 mPas [27,28], while at the same temperature the viscosities of MEA and 2-methoxyethanol are 24.1 mPas [29,30] and 1.71 mPas [31] respectively.

The precursor solution was found to be stable, in that it did not produce any precipitate even after 30 days of storage at ambient temperature. However, in practice, the solution was used for coating immediately after stirring. The solution was placed on a 1 mm thick indium tin oxide (ITO)-coated glass substrate (Corning Inc. 7059 alkali-free borosilicate glass, size

25 mm × 25 mm) and spun at 2500 rpm for 30 s in a spin coater (spinNXG-P1, Apex Instruments Co. Pvt. Ltd., India), to form precursor thin films. The films were then heated at the temperature of 190–195 °C in air for 20 min in an oven to remove the solvent and the organic residuals, leaving the deposited film as a gel. The coating and the heating process was repeated a number of times to obtain zinc oxide-based films of sufficient thickness. Repeated trials of film production found that depositing 20–25 layers gave rise to homogeneous films on the substrate after subsequent heat treatment, rather than films which broke down into islands after the subsequent crystallisation heat treatment. Part of the ITO substrate was masked off during this deposition procedure for electrical contact to be made subsequently with the ITO side of the zinc-oxide-based thin film. For the subsequent crystallisation procedure, the films were annealed in air at either 550 °C or 700 °C for 1 h. The rate of heating to the annealing temperature was 10 °C min^{-1}.

Crystallisation of the thin film samples was examined by an X-ray powder diffractometer (BRUKER D8) using CuK_α radiation (λ = 0.15405 nm). The X-ray diffraction patterns were recorded in a scan mode with an angular step size of 0.02° $\Delta 2\theta$ and a 1 s dwell time at each step.

The morphologies of the surface of the thin films and cross-sections of the films were examined by scanning electron microscopy using a JEOL JSM-6340F scanning electron microscope at 30 kV. The chemical composition of the film surfaces was estimated by energy dispersive X-ray analysis (EDAX) at 20 kV on a FEI Quanta 200F field emission gun scanning electron microscope.

The current (I) – voltage (V) characteristics of the thin films were studied with a programmable source meter (Keithley 2400). A voltage step of 0.1 V was used for the current measurements. The data for I–V characteristics were collected at different regions on the film surfaces using a 10 mm square electrode area. Prior to the electrical measurements, gold was sputter coated onto the thin films to provide the electrical contact required on the top surface of the film. Electrical contact was established to the meter and the source voltage through simple pressure contacts between connecting wires and (i) the area masked off on the ITO side during the zinc-oxide-based thin film deposition and (ii) the gold coating.

Further electrical measurements were undertaken on the same films using a HIOKI 3532-50 LCR HiTester at room temperature. This tester was used for both impedance spectroscopy measurements and capacitance–voltage measurements. In each case the electrodes were 15 mm square in size. An AC impedance spectrum in the frequency range

42 Hz – 100 kHz was measured at room temperature. The signal level for the impedance measurements was 10 mV. For the capacitance–voltage measurements, capacitance measurements were taken at a frequency of 100 kHz as the voltage was altered from 0 to 5 V.

3. Results and Discussion

3.1. X-ray diffraction patterns

X-ray diffraction patterns over the angular range 10 – 80° 2θ of a borosilicate glass slide without ITO and one with ITO after a 1 h heat treatment at 550 °C are shown in Fig. 1. These X-ray diffraction patterns were used as standards with which to compare the X-ray diffraction patterns of the zinc oxide-coated ITO-coated glass slides. It is apparent from Fig. 1(a) that the borosilicate glass slide exhibits an X-ray diffraction pattern consistent with it being amorphous, with the increase in intensity peaking at 25° 2θ characteristic of silicate-based inorganic glasses. Heat treatment of ITO-coated borosilicate glass produces crystallisation of the coating (Fig. 1(b)). Analysis of the diffraction peaks shows that these can all be attributed to indium sesquioxide, In_2O_3. Pure In_2O_3 has the cubic bixbyite crystal structure (space group $Ia\bar{3}$, no. 206) with a = 10.117 Å [32]. Typically, ITO coatings are 10 wt% SnO_2 – 90 w% In_2O_3 in composition, produced by a variety of methods [33]. 50 nm thick ITO films produced by electron beam evaporation can fully crystallise when held at 162 °C for 1 h, resulting in block-like grains 100 nm in size by a nucleation and growth process and a marked reduction in resistivity of the ITO film [33]. Others have also reported results of heat treatment of 250 nm think ITO films for 1 h at 350–550 °C [34], in which many sub-micron crystallites of indium sesquioxide of different orientations and sizes are produced as a result of nucleation and growth processes, embedded in an amorphous matrix from the originally evaporated ITO thin film.

X-ray diffraction patterns of the zinc-oxide-based thin films deposited on the ITO-coated glass slides over the angular range 10 – 80° 2θ of the thin films annealed at 550 °C and 700 °C are shown in Figs. 2(a) and 2(b) respectively. Analyses of these diffraction patterns shows that the diffraction peaks seen in both X-ray diffraction patterns can be attributed to indium sesquioxide, In_2O_3, and ZnO. Peaks labelled in blue in Fig. 2(a) are from In_2O_3, while peaks labelled in red are from ZnO. Pure ZnO has the wurtzite crystal structure (space group $P6_3mc$, no. 186) and is hexagonal with a = 3.250 Å and c = 5.207 Å [35]. It is evident that the 411 In_2O_3 peak clearly visible in Fig. 1(a) is seen as a minor shoulder of the 101 ZnO peak in Fig. 2(a) and as a small separate peak at a 2θ value of 37.7° in Fig. 2(b).

The average grain size estimated from the full width half maxima of the higher intensity ZnO peaks in Fig. 1(b) from the (100), (101) and (002) planes is 75 nm.

These ZnO films do not have either a noticeable *c*-axis texture or a noticeable *a*-axis texture that have been reported by others and are summarised in the recent review on sol–gel deposited ZnO films by Znaidi [19]. Instead, the peak intensities are in accord with reference ICDD powder diffraction patterns such as 01-071-2194 for In_2O_3 and 01-070-8072 for ZnO. The reason for this can be attributed to the concurrent crystallisation of the ITO coating during the annealing heat treatments of the sol–gel deposited films preventing the development of a noticeable texture in the ZnO films.

There are a number of secondary phases reported in the ZnO–V_2O_5 binary oxide system such as $Zn_4V_2O_9$, $Zn_3V_2O_8$ and $Zn_2V_2O_7$ [36]. The presence of manganese oxide in the starting composition complicates this situation further [37], so that for example phases such as the *L* phase, $(Mn,Zn)_2V_2O_7$, are also possible secondary phases [26,38]. However, no evidence for the presence of any of these phases was found in the X-ray diffraction patterns. Therefore, if such phases are formed, it can be concluded that their amounts are each below the detection limit in X-ray diffraction. It is also relevant that In_2O_3 and ZnO only react above 1000 °C [39], i.e., at temperatures far higher than the annealing temperatures we have used in this work.

3.2. Microstructural observations

Scanning electron micrographs of an oxide thin film annealed at 700 °C are shown in plan view and transverse view in Fig. 3(a) and 3(b) respectively. The film is seen to be composed of nanocrystalline grains densely packed, although there is some evidence of porosity. An average grain diameter of 37 nm was estimated from the plan view in Fig. 3(a) by Image J software, half that estimated from the full width half maxima of the ZnO X-ray diffraction peaks. Attempting to count the number of grains in transverse view was unreliable – it was evident that what appeared to be separate grains was instead the consequence of film porosity, favouring non-planar surface sections. However, it is apparent from the transverse view of the film in Fig. 3(b) that the film thickness is approximately 250 nm, so that across the film there are on average about 3–7 grains. It is also noteworthy in Fig. 3(a) that there are many neighbouring grains of the order of 75 nm in size. This is relevant to the flow of electric current through these thin films – the current will choose the optimum path, i.e., the

path of least resistance, so that presence of large grains will dominate the *I–V* film characteristics [3].

Results from X-ray microanalysis of an area of thin film annealed at 700 °C seen in plan view is shown in Fig. 4. The chemical composition inferred from this area confirms the presence of both vanadium and manganese in the film and is in good agreement with the target composition of the film material, although, significantly, it is evident that there is more vanadium and less manganese than expected in the film.

3.3. I–V characteristics

Electrical contact for *I–V* measurements of the films was achieved through having the crystallised ITO coating on the borosilicate glass substrate side of the film and an evaporated gold film on the other. Crystallisation of the ITO coating reduces its electrical resistivity relative to amorphous ITO deposited at room temperature under low kinetic energy deposition methods [33,34]. However, in our work, we found that there was a slight increase in the electrical resistivity of the ITO coating deposited on the ZnO substrate The crystallisation of the ITO was useful in helping to interpret the *I–V* measurements in terms of the dominant behaviour of the zinc oxide thin film [33,34].

An example of an *I–V* characteristic obtained from a film annealed at 700°C is shown in Fig. 5, plotted in linear coordinates in (a) and logarithmically in (b) for values of current between 0.19 nA and 1.23 μA. Varistor action is readily seen in (a). When plotted logarithmically (Fig. 5(b)), it is evident that varistor action starts at a voltage as low as 2 V. Over the range 0.19 nA – 1.23 μA the non-linear coefficient, α, in the assumed power law relationship $I \propto V^{\alpha}$ [3] is relatively modest: $1/0.229 \cong 4.4$, but this demonstrates convincingly the proof of principle of varistor action in these thin films. An average breakdown voltage per boundary of the order of 0.6 V, on the basis of a breakdown voltage of 2 V and three grain boundaries traversed through the thickness of the film, is a realistic order-of-magnitude estimate: electric current will choose the least resistive path across a thin film and so choose a path with as few grain boundaries as possible across the film [3]. Therefore, the porosity evident in Fig. 3(a) will not have an effect on the *I–V* characteristics of these varistor thin films.

In a recent study on bulk $ZnO–V_2O_5$ varistors doped with MnO_2, PbO and a mixture of MnO_2, PbO and B_2O_3, Wu et al. [40] reported an α value of 4.2 and a breakdown field of

106.1 V mm^{-1} for their ZVM sample containing 98.5 mol% ZnO, 0.5 mol% V_2O_5 and 1 mol % MnO_2. The grain size quoted for this bulk varistor was 14.2 μm, implying an average breakdown voltage per boundary of the order of 1.5 V per boundary. While this is higher than the value we have estimated here for our varistor thin films, it is not that dissimilar.

3.4 Impedance Spectrum

The AC impedance spectrum for the ZnO–based thin film from which the *I*–*V* measurements shown in Fig. 5 were made is shown in Fig. 6. As Moulson and Herbert discuss [41], there are a number of equivalent circuit models that can be used to identify the characteristics of 'lossy' capacitors, i.e., materials with both a resistive and a capacitive component. For bulk devices where there is good electrode contact, it is usual to describe a ZnO varistor in terms of a bulk resistance representing ZnO grains in series with a parallel combination of a resistor and capacitor representing the grain boundary component (e.g., Fig. 7 of [40]).

However, it is evident from Fig. 6 that for this thin film, a material expected to have a relatively low resistance relative to a bulk ZnO varistor, account needs to be taken of the electrode-varistor interfacial regions as well. The impedance spectrum would seem to be dominated by the relatively poor quality of the contact of the electrodes because the maximum in Z'' is no more than 0.3 MΩ, while the maximum in Z' as the angular frequency $\omega \rightarrow 0$ is close to 3 MΩ. It is therefore reasonable to interpret this data in terms of a contribution to the total value of Z' of the grain boundary resistance in the thin film to be no more than 0.3 MΩ, with the remainder of the contribution to Z' as $\omega \rightarrow 0$ due to poor electrode contact. Hence, for a 250 nm thick film, t, and an electrode area, A, of $0.225\times10^{-3}\,m^2$, the grain boundary resistivity, ρ_{gb}, is estimated to be $0.3A/t$ MΩ m = 270 MΩ m. While large, this is of a similar magnitude to the 8089 MΩ cm (80.89 Ω m) reported by Wu et al. [40] for a ZnO bulk varistor doped with 0.5 mol.% V_2O_5 + 1.0 mol.% MnO_2 + 2.3 mol.% PbO + 1.7 mol.% B_2O_3.

3.5 C–V measurements

Under suitable circumstances, *C*–*V* measurements are able to determine average donor concentrations, N_d, and barrier heights φ at grain boundaries in bulk ZnO-based varistors

[42,43]. However, as Alim et al. show, at low applied voltages over a range of frequencies for bulk varistors, the expected capacitance–voltage relationship may not be observed experimentally, and instead, within experimental error at low voltages, the capacitance is linear with voltage before decreasing as the voltage is increased [44]. Alim et al. interpreted the behaviour in bulk varistors that they observed in terms of parallel trapping relaxation events with respect to the true barrier layer capacitance at prebreakdown voltage levels. We found this to be the case with the *C–V* measurements we undertook on the sample from which Figs. 5 and 6 were taken. At these low voltages, the measured capacitance of the thin film was 2.6 μF, independent of the voltage applied within the range 0 – 5 V. Relating this measured capacitance to the capacitance per unit area of grain boundary in the theory of Mukae et al. [42, 43] using a value for the relative permittivity of pure ZnO of 8 gives a ratio N_d/φ of the order of 10^{27} m^{-3} V^{-1}. Since values of φ are considered to be about 1 V [42], this implies a high donor concentration in these thin films of the order of 10^{27} m^{-3}; while high, this value compares with a concentration of Zn ions m^{-3} in stoichiometric ZnO of 4.2×10^{28} m^{-3}.

4. Conclusions

Convincing evidence for varistor action in the Zn–V–Mn–O system in thin films prepared by a sol–gel process has been found. The advantages of a sol-gel deposition procedure are that it gives good compositional homogeneity, and that it is inexpensive and easy to prepare. It is evident from this preliminary work that there is scope for further optimisation of these sol–gel deposited thin films in terms of the thickness of the resultant thin films after multiple deposition procedures. One key variable to be explored is the reproducibility of the microstructure; a second is the optimisation of chemical composition within the Zn–V–Mn–O system and other systems, and a third is the ability to produce robust electrical contacts. Clarke [3] noted that thin films are expected to have an intrinsically lower nonlinearity coefficient than bulk materials of the same nominal overall composition, and a greater vulnerability to puncture failure. This is an obvious avenue to pursue in future work on this and other systems.

Acknowledgements

Two of the authors (AS and KMK) wish to acknowledge the British Council, New Delhi for providing financial support for this work through UKIERI project SA07-0052.

References

[1] M. Matsuoka, Nonohmic properties of zinc oxide ceramics, Jpn. J. Appl. Phys. 10 (1971) 736–746.

[2] N. Horio, M. Hiramatsu, M. Nawata, K. Imaeda, T. Torii, Preparation of zinc oxide/metal oxide multilayered thin films for low-voltage varistors, Vacuum 51 (1998) 719–722.

[3] D.R. Clarke, Varistor ceramics, J. Am. Ceram. Soc. 82 (1999) 485–502.

[4] L.M. Levinson, H.R. Philipp, Zinc oxide varistors – a review, Am. Ceram. Soc. Bull. 65 (1986) 639–646.

[5] J.-K. Tsai, T.-B. Wu, Microstructure and nonohmic properties of binary ZnO–V_2O_5 ceramics sintered at 900°C, Mater. Lett. 26 (1996) 199–203.

[6] J.-K. Tsai, T.-B. Wu, Non-ohmic characteristics of ZnO-V_2O_5 ceramics, J. Appl. Phys. 76 (1994) 4817–4822.

[7] C.-T. Kuo, C.-S. Chen, I.-N. Lin, Microstructure and nonlinear properties of microwave-sintered ZnO–V_2O_5 varistors: I, Effect of V_2O_5 doping, J. Am. Ceram. Soc. 81 (1998) 2942–2948.

[8] C.-T. Kuo, C.-S. Chen, I.-N. Lin, Microstructure and nonlinear properties of microwave-sintered ZnO–V_2O_5 varistors: II, Effect of Mn_3O_4 doping, J. Am. Ceram. Soc. 81 (1998) 2949–2956.

[9] H.H. Hng, K.M. Knowles, Characterisation of $Zn_3(VO_4)_2$ phases in V_2O_5-doped ZnO varistors, J. Eur. Ceram. Soc. 19 (1999) 721–726.

[10] H.H. Hng, L. Halim, Grain growth in sintered ZnO–1 mol% V_2O_5 ceramics, Mater. Lett. 57 (2003) 1411–1416.

[11] Y.Q. Huang, L. Meidong, Z. Yike, L. Churong, X. Donglin, L. Shaobo, Preparation and properties of ZnO-based ceramic films for low-voltage varistors by novel sol-gel process, Mater. Sci. Eng. B 86 (2001) 232–236.

[12] J.B. Miller, H.-J. Hsieh, B.H. Howard, E. Broitman, Microstructural evolution of sol–gel derived ZnO thin films, Thin Solid Films, 518 (2010) 6792–6798.

[13] M. Ohyama, H. Kozuka, T. Yoko, Sol-gel prepration of ZnO films with extremely preferred orientation along (002) plane from zinc acetate solution, Thin Solid Films 306 (1997) 78–85.

[14] J.-H. Lee, K.-H. Ko, B.-O. Park, Electrical and optical properties of ZnO transparent conducting films by the sol–gel method, J. Cryst. Growth 247 (2003) 119–125.

[15] J.-H. Lee, B.-W. Yeo, B.-O. Park, Effects of the annealing treatment on electrical and optical properties of ZnO transparent conduction films by ultrasonic spraying pyrolysis, Thin Solid Films 457 (2004) 333–337.

[16] E. Hosono, S. Fujihara, T. Kimura, H. Imai, Growth of layered basic zinc acetate in methanolic solutions and its pyrolytic transformation into porous zinc oxide films, J. Coll. Interface Sci. 272 (2004) 391–398.

[17] E. Hosono, S. Fujihara, T. Kimura, Fabrication and electrical properties of micro/nanoporous ZnO : Al films, J.Mater.Chem. 14 (2004) 881–886.

[18] Y.-S. Kim, W.-P. Tai, S.-J. Shu, Effect of preheating temperature on structural and optical properties of ZnO thin films by sol–gel process, Thin Solid Films 491 (2005) 153–160.

[19] L. Znaidi, Sol–gel–deposited ZnO thin films: A review, Mater. Sci. Eng. B 174 (2010) 18–30.

[20] N.R.S. Farley, C.R. Staddon, L. Zhao, K.W. Edmonds, B.L. Gallagher, D.H. Gregory, Sol-gel formation of ordered nanostructured doped ZnO films, J. Mater. Chem.14 (2004) 1087–1092.

[21] D. Bao, H. Gu, A. Kuang, Sol–gel-derived *c*-axis oriented ZnO thin films, Thin Solids Films 312 (1998) 37–39.

[22] H.H. Hng, K.M. Knowles, Microstructure and current–voltage characteristics of multicomponent vanadium-doped zinc oxide varistors, J. Am. Ceram. Soc. 83 (2000) 2455–2462.

[23] H.H. Hng, K.M. Knowles, P.A. Midgley, Zinc vanadates in vanadium oxide-doped zinc oxide varistors, J. Am. Ceram. Soc. 84 (2001) 435–441.

[24] H. Pfeiffer, K.M. Knowles, Effects of vanadium and manganese concentrations on the composition, structure and electrical properties of ZnO-rich MnO_2–V_2O_5–ZnO varistors , J. Eur. Ceram. Soc., 24 (2004) 1199–1203.

[25] C.-S. Chen, Effect of dopant valence state of Mn-ions on the microstructures and nonlinear properties of microwave sintered ZnO-V_2O_5 varistors, J. Mater. Sci., 38 (2003) 1033–1038.

[26] K.M. Knowles, M.E. Vickers, A. Sil, Y.-H. Han, P. Jaffrenou, X-ray powder diffraction and electron diffraction studies of the thortveitite-related *L* phase, $(Zn,Mn)_2V_2O_7$, Acta Cryst. B, 65 (2009) 160–166.

[27] N.G. Tsierkezos, I.E. Molinou, Thermodynamic properties of water + ethylene glycol at 283.15, 293.15, 303.15, and 313.15 K, J. Chem. Eng. Data, 43 (1998) 989–993.

[28] C-S. Yang. P-S. Ma, F-M. Jing, D-Q. Tang, Excess molar volumes, viscosities, and heat capacities for the mixtures of ethylene glycol + water from 273.15 to 353.15 K, J. Chem. Eng. Data, 48 (2003) 836–840.

[29] B.P. Mandal, M. Kundu, S.S. Bandyopadhyay, Density and viscosity of aqueous solutions of (*N*-methyldiethanolamine + monoethanolamine), (*N*-methyldiethanolamine + diethanolamine), (2-amino-2-methyl-1-propanol + monoethanolamine), and (2-amino-2-methyl-1-propanol + diethanolamine), J. Chem. Eng. Data, 48 (2003) 703–707.

[30] U.S.P.R. Arachchige, N. Aryal, D.A. Eimer, M.C. Melaaen, Viscosities of pure and aqueous solutions of monoethanolamine (MEA), diethanolamine (DEA) and N-methyldiethanolamine (MDEA), Ann. Trans. Nordic Rheol. Soc., 21 (2013) 299–306.

[31] C.M. Kinart, W.J. Kinart, A. Ćwiklińska, Density and viscosity at various temperatures for 2-methoxyethanol + acetone mixtures, J. Chem. Eng. Data, 47 (2002) 76–78.

[32] M. Marezio, Refinement of the crystal structure of In_2O_3 at two wavelengths, Acta Cryst., 20 (1966) 723–728.

[33] D.C. Paine, T. Whitson, D. Janiac, R. Beresford, C.O. Yang, B. Lewis, A study of low temperature crystallization of amorphous thin film indium–tin–oxide, J. Appl. Phys. 85 (1999) 8445–8450.

[34] H.R. Fallah, M. Ghasemi, A. Hassanzadeh, Influence of heat treatment on structural, electrical, impedance and optical properties of nanocrystalline ITO films grown on glass at room temperature prepared by electron beam evaporation, Physica E 39 (2007) 69–74.

[35] J.Albertsson, S.C. Abrahams, Å. Kvick, Atomic displacement, anharmonic thermal vibration, expansivity and pyroelectric coefficient thermal dependences in ZnO, Acta Cryst. B 45 (1989) 34–40.

[36] M. Kurzawa, I.Rychlowska-Himmel, M. Bosacka, A. Blonska-Tabero, Reinvestigation of phase equilibria in the V_2O_5–ZnO system, J. Therm. Anal. Cal. 64 (2001) 1113–1119.

[37] L.L. Surat, V.D. Zhuravlev, A.A. Fotiev, Y.A. Velikodnyi, Phase relations in MO-M'O-V_2O_5 (M, M' = Cd, Zn, Ni, Mn) systems, Zh. Neorg. Khim. 41 (1996) 1370–1372. [English translation, Russian Journal of inorganic Chemistry, 41 (1996) 1311–1313.]

[38] T.I. Krasnenko, M.V. Rotermel, L.V. Zolotukhina, L.G. Maksimova, R.G. Zakharov, Phase equilibria of the $Mn_2V_2O_7$–$Zn_2V_2O_7$ system, Zh. Neorg. Khim. 47 (2002) 1888–1891. [English translation, Russian Journal of inorganic Chemistry, 47 (2002) 1737–1740.]

[39] T. Moriga, D.D. Edwards, T.O. Mason, G.B. Palmer, K.R. Poeppelmeier, J.L. Schindler, C.R. Kannewurf, I. Nakabayashi, Phase relationships and physical properties of homologous compounds in the zinc oxide–indium oxide system, J. Am. Ceram. Soc. 81 (1998) 1310–1316.

[40] J. Wu, T.-T. Li, T. Qi, Q.-W. Qin, G.-Q. Li, B.-L. Zhu, R. Wu, C.S. Xie, Influence of dopants on electrical properties of ZnO-V_2O_5 varistors deduced from AC imperdance and variable-temperature dielectric spectroscopy, J. Elect. Mater. 41 (2012) 1970–1977.

[41] A.J. Moulson, J.M. Herbert, Electroceramics, second ed., Wiley, Chichester, U.K., 2003.

[42] K. Mukae, K. Tsuda, I. Nagasawa, Capacitance-vs-voltage characteristics of ZnO varistors. J. Appl. Phys. 50 (1979) 4475–4476.

[43] P.R. Bueno, J.A. Varela, E. Longo, SnO_2, ZnO and related polycrystalline compound semiconductors: An overview and review on the voltage-dependent resistance (non-ohmic) feature, J. Eur. Ceram. Soc. 28 (2008) 505–529.

[44] M.A. Alim, M.A. Seitz, R.W. Hirthe, Complex plane analysis of trapping phenomena in zinc oxide based varistor grain boundaries, J. Appl. Phys. 63 (1988) 2337–2345.

Figure Captions

Fig. 1 XRD patterns of (a) borosilicate glass and (b) ITO-coated borosilicate glass annealed for 1 hr at 550 °C.

Fig. 2. XRD patterns of ZnO-based films annealed for 1 h at (a) 550 °C and (b) 700 °C. Peaks labelled in blue in (a) are from In_2O_3; peaks labelled in red are from ZnO.

Fig. 3. (a) Plan view and (b) transverse view scanning electron micrographs of the thin film annealed at 700 °C for 1 h. The ZnO thin film is highlighted by the two thin horizontal white lines in (b).

Fig. 4. Energy dispersive X-ray analysis of a thin film sample annealed for 1 h at 700 °C, together with chemical compositions determined using *ZAF* correction factors.

Fig. 5. *I*–*V* characteristic obtained from a film annealed at 700 °C for 1 h. (a) linear plot of voltage against current, together with detail in the inset for $V < 5$ V, (b) logarithmic plot of voltage against current between current values of 0.19 nA and 1.23 μA.

Fig. 6. AC impedance spectrum of the ZnO thin film tested at room temperature from which the *I*–*V* characteristic in Fig. 5 was obtained.

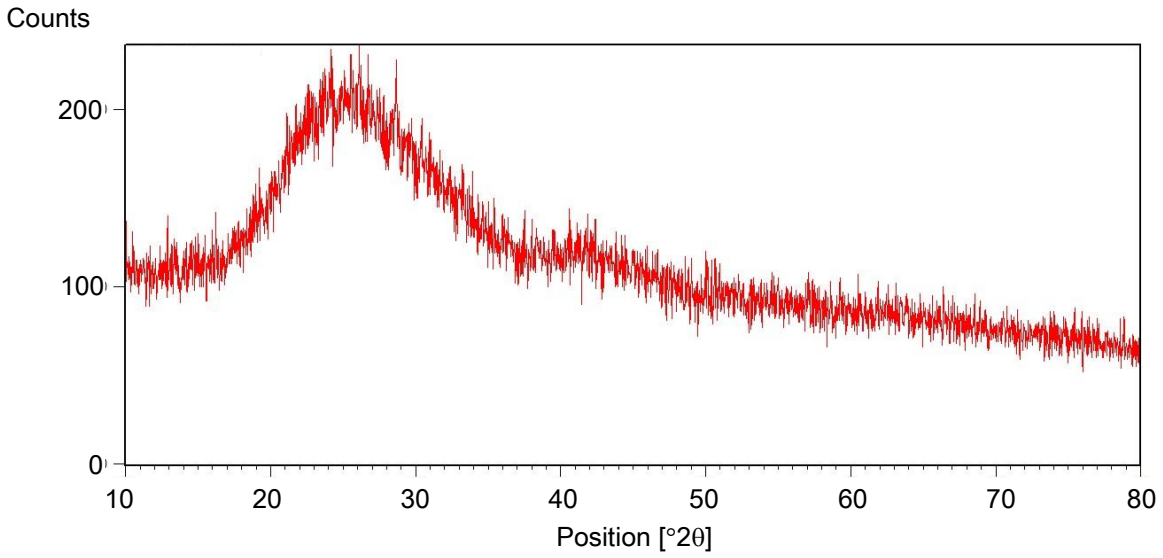

(a)

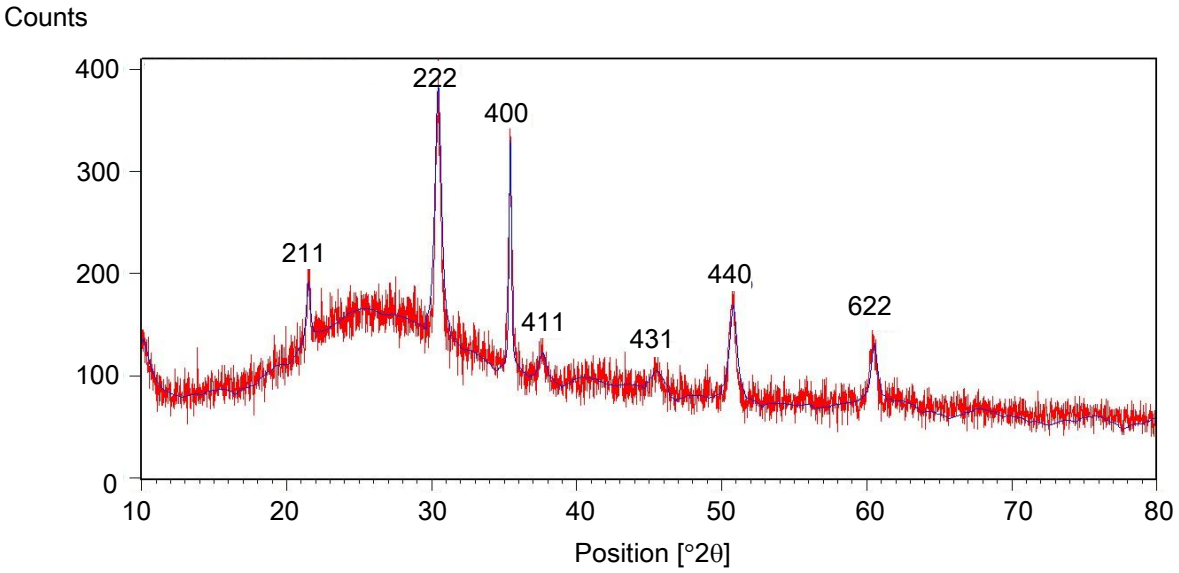

(b)

Fig. 1. XRD patterns of (a) borosilicate glass and (b) ITO-coated borosilicate glass annealed for 1 hr at 550 °C.

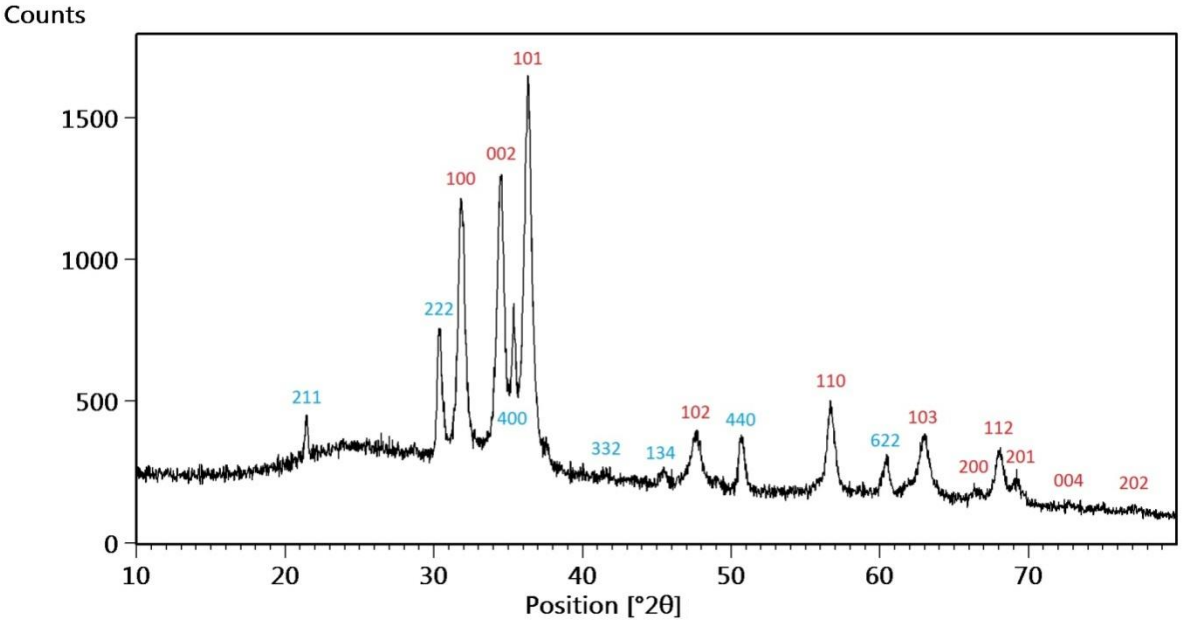

(a)

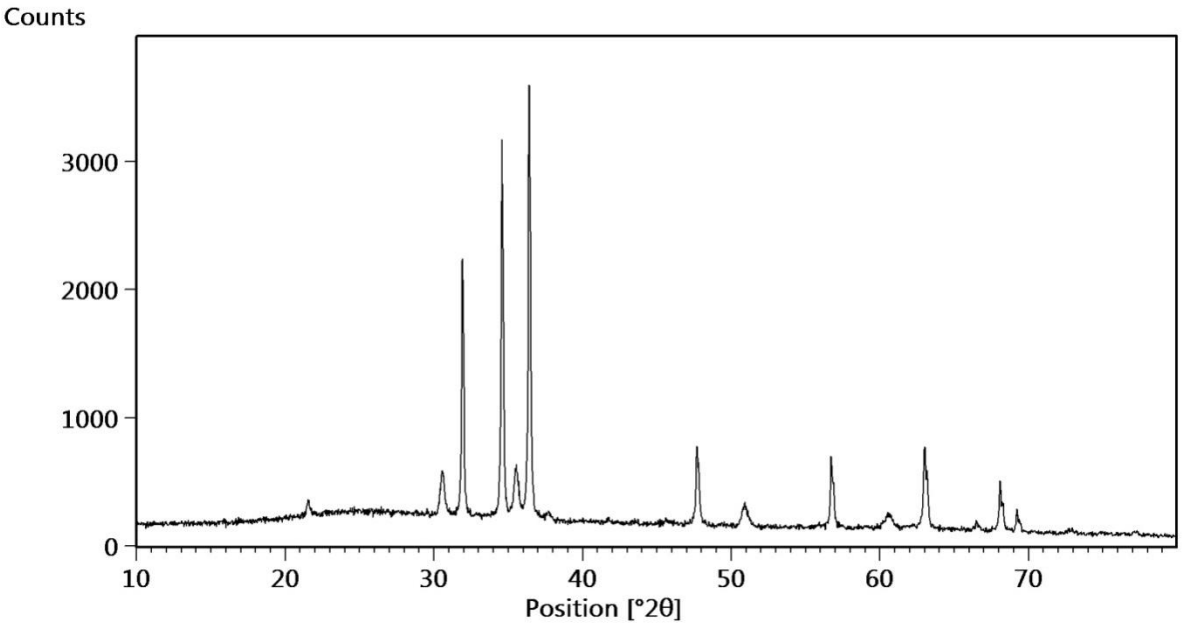

(b)

Fig. 2. XRD patterns of ZnO-based films annealed for 1 h at (a) 550 °C and (b) 700 °C. Peaks labelled in blue in (a) are from In_2O_3; peaks labelled in red are from ZnO.

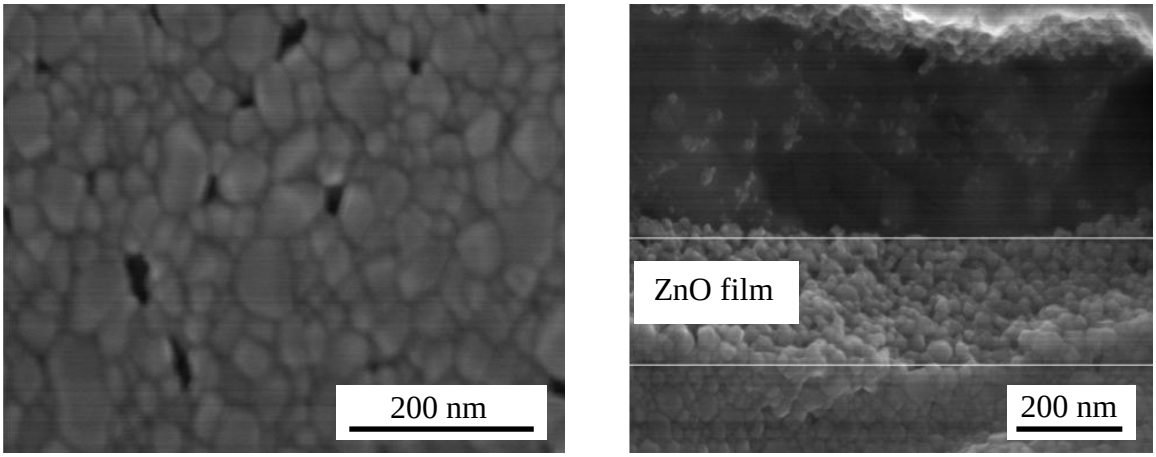

(a) (b)

Fig. 3. (a) Plan view and (b) transverse view scanning electron micrographs of the thin film annealed at 700 °C for 1 h. The ZnO thin film is highlighted by the two thin horizontal white lines in (b).

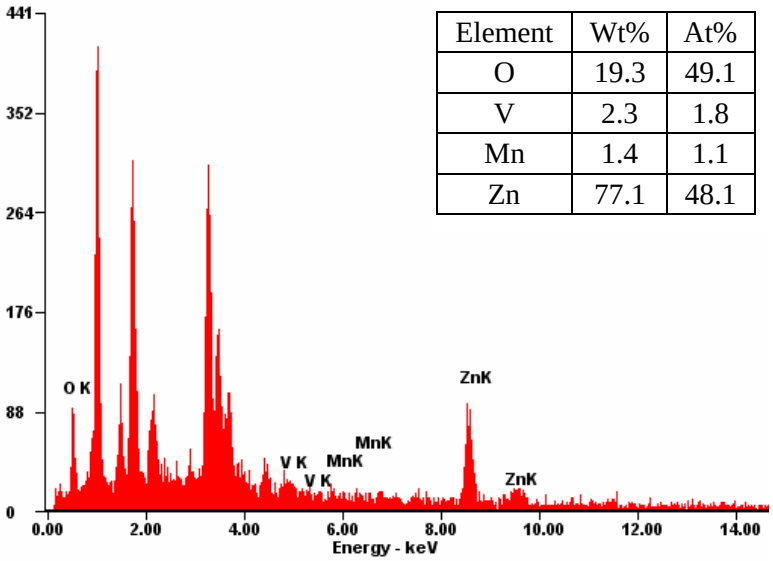

Element	Wt%	At%
O	19.3	49.1
V	2.3	1.8
Mn	1.4	1.1
Zn	77.1	48.1

Fig. 4. Energy dispersive X-ray analysis of a thin film sample annealed for 1 h at 700 °C, together with chemical compositions determined using *ZAF* correction factors.

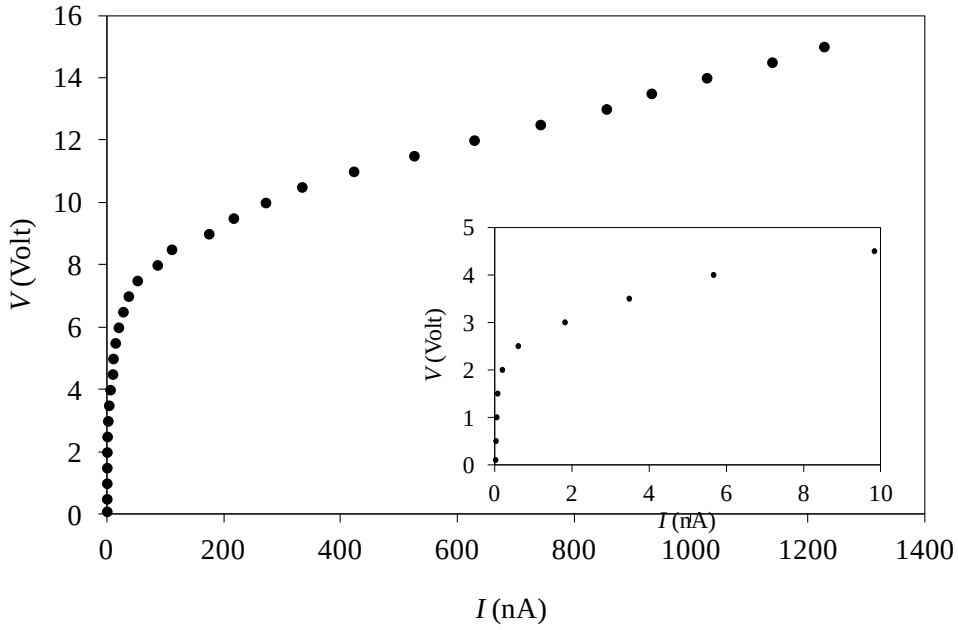

(a)

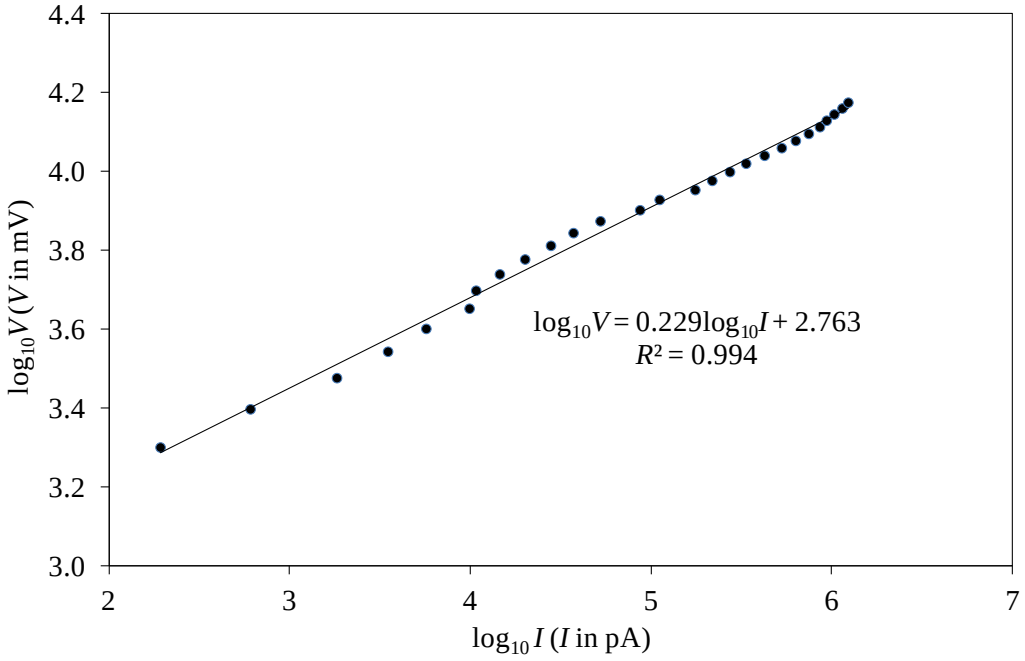

(b)

Fig. 5. *I*–*V* characteristic obtained from a film annealed at 700 °C for 1 h. (a) linear plot of voltage against current, together with detail in the inset for $V < 5$ V, (b) logarithmic plot of voltage against current between current values of 0.19 nA and 1.23 μA.

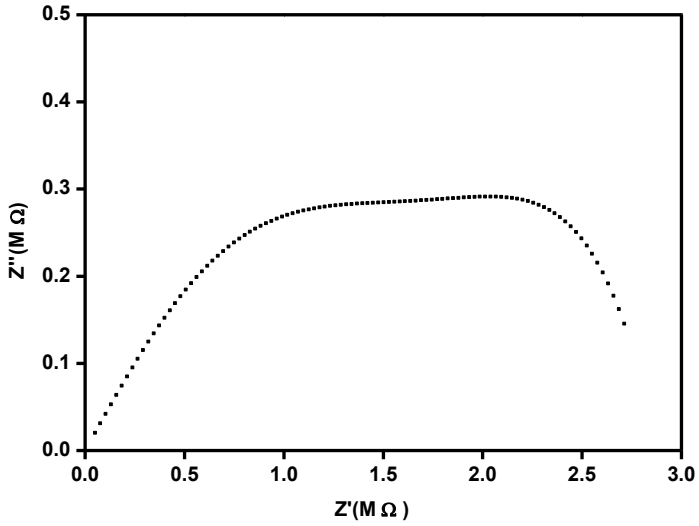

Fig. 6. AC impedance spectrum of the ZnO thin film tested at room temperature from which the *I*–*V* characteristic in Fig. 5 was obtained.